



On the derivation of
particle nucleation
rates from
experimental
formation rates

A. Kürten et al.

This discussion paper is/has been under review for the journal Atmospheric Chemistry and Physics (ACP). Please refer to the corresponding final paper in ACP if available.

On the derivation of particle nucleation rates from experimental formation rates

A. Kürten¹, C. Williamson¹, J. Almeida², J. Kirkby^{1,2}, and J. Curtius¹

¹Institute for Atmospheric and Environmental Sciences, Goethe University of Frankfurt, Frankfurt, Germany

²CERN, Geneva, Switzerland

Received: 8 October 2014 – Accepted: 14 October 2014 – Published: 29 October 2014

Correspondence to: A. Kürten (kuerthen@iau.uni-frankfurt.de)

Published by Copernicus Publications on behalf of the European Geosciences Union.

Title Page

Abstract

Introduction

Conclusions

References

Tables

Figures



Back

Close

Full Screen / Esc

Printer-friendly Version

Interactive Discussion



**On the derivation of
particle nucleation
rates from
experimental
formation rates**

A. Kürten et al.

Title Page

Abstract

Introduction

Conclusions

References

Tables

Figures

◀

▶

◀

▶

Back

Close

Full Screen / Esc

Printer-friendly Version

Interactive Discussion

Until recently the smallest mobility diameter that could be measured by a condensation particle counter (CPC) was 2.5 to 3 nm – which is substantially larger than the critical size. However, the detection limit of newly-developed CPCs is as small as 1.2 nm (Sgro and Fernández de la Mora, 2004; Iida et al., 2009; Vanhanen et al., 2011; Kuang et al., 2012a; Wimmer et al., 2013). Nevertheless, despite this progress the most widely-used CPCs have detection thresholds at 2.5 nm or above. Moreover, care is needed when interpreting data from the newly-developed CPCs since they can be sensitive to the chemical composition of the particles (Kangasluoma et al., 2014). Furthermore, CPC cut-off curves do not have the shape of a step function. Instead, detection of particles below the cut-off size (usually defined as the size d_{50} , where 50 % of the particles are detected) is occurring to some extent and, if this includes clusters below the critical size, the accuracy of the derived nucleation rates can be strongly affected. For this reason, under certain conditions, it can still be more reliable to use a conventional CPC with a nominal cut-off around 3 nm for determining NPF rates. On the other hand, in order to minimize the corrections, it is advantageous to measure the formation rates as close as possible to the critical size.

Kerminen and Kulmala (2002) have derived an analytical formula for correcting experimental particle formation rates to determine nucleation rates at a given critical size (abbreviated as the KK method in the following). This method was developed for atmospheric nucleation measurements and a similar formula was also used by the McMurry group (Weber et al., 1997; McMurry et al., 2005). In addition to atmospheric measurements, nucleation studies in aerosol chambers or flow reactors have tremendously helped the understanding of aerosol nucleation. Such experiments require an accurate method to derive the NPF rates. In this study the applicability of the KK method to chamber experiments such as CLOUD (Cosmics Leaving Outdoor Droplets) at CERN will be examined (Kirkby et al., 2011; Almeida et al., 2013; Riccobono et al., 2014). It is shown that KK has limited applicability for chamber nucleation studies, and an alternative method is needed. We therefore present here a new method that yields accurate results for any environment – be they chamber or atmospheric data – provided the

particle size distribution above a certain threshold size is known, as well as the particle growth rate, and where all loss processes are quantified as a function of size. The new method is verified with the results from a kinetic aerosol model.

2 Methods

2.1 Review of the KK method

KK make the following assumptions in deriving their formulae (Kerminen and Kulmala, 2002):

1. the only important sink for new particles is their coagulation with larger pre-existing particles,
2. the new particles grow at a constant rate, and
3. the population of pre-existing particles remains unchanged during the new particle growth.

We will assume for now that assumption 2 is fulfilled, although the particle growth rate could be a function of size (Kuang et al., 2012b; Kulmala et al., 2013). Section 3.1 will deal with this question. Assumption 1 is generally true for the atmosphere, for which KK was derived. However, for chamber experiments, the losses due to walls and dilution are not equivalent and, as we shall see later, this introduces considerable inaccuracies. Assumption 3 is not fulfilled since self-coagulation can become important when formation rates are large (see also Anttila et al., 2010). However, the main reason for the failure of KK when applied to chamber studies is not assumption 3 but rather an approximation made that is only valid under certain conditions (see below).

On the derivation of
particle nucleation
rates from
experimental
formation rates

A. Kürten et al.

Title Page

Abstract

Introduction

Conclusions

References

Tables

Figures



Back

Close

Full Screen / Esc

Printer-friendly Version

Interactive Discussion

Let's start by deriving the KK formulae according to their paper. Assumption 1 can be written as:

$$\frac{dN(d_p)}{dt} = -N(d_p) \cdot \sum_j K(d_p, d_j) \cdot N_j \quad (1)$$

5 which means that the change in particle concentration N at particle size d_p can be described by the coagulation with larger particles in the size bins j , where K is the collision rate between particles of size d_p and d_j , and N_j is the concentration of particles in size bin j . Equation (1) can also be written as

$$\frac{dN(d_p)}{dt} = \frac{dN(d_p)}{dd_p} \cdot \frac{dd_p}{dt} \quad (2)$$

10 where dd_p/dt is the growth rate (GR), which is constant according to assumption 2. Therefore Eq. (1) becomes

$$\frac{dN(d_p)}{dd_p} = -\frac{N(d_p)}{GR} \cdot \sum_j K(d_p, d_j) \cdot N_j \quad (3)$$

15 Rearranging yields:

$$\frac{dN(d_p)}{N(d_p)} = -\frac{1}{GR} \cdot \sum_j K(d_p, d_j) \cdot N_j \cdot dd_p \quad (4)$$

20 The left-hand side (LHS) can be integrated from $N(d_{p1})$ to $N(d_{p2})$ (e.g. mobility diameters of $d_{p1} = 1.7$ nm and $d_{p2} = 3.2$ nm). However, the dependency of the collision rate K on d_p , on the right-hand side (RHS) of the equation, cannot be analytically integrated. Therefore, KK made the following assumption (this is actually the important approximation) that

$$K(d_p, d_j) \cdot d_p^2 = K(d_0, d_j) \cdot d_0^2 \quad (5)$$

On the derivation of particle nucleation rates from experimental formation rates

A. Kürten et al.

Title Page	
Abstract	Introduction
Conclusions	References
Tables	Figures
◀	▶
◀	▶
Back	Close
Full Screen / Esc	
Printer-friendly Version	
Interactive Discussion	



and chose $d_0 = 1$ nm. This last equation assumes that the collision rate decreases with particle size to the second power. Making this assumption Eq. (4) can be written as

$$\frac{dN(d_p)}{N(d_p)} = -\frac{1}{GR} \cdot \frac{d_0^2}{d_p^2} \cdot \sum_j K(d_0, d_j) \cdot N_j \cdot dd_p \quad (6)$$

5 and the RHS can now be analytically integrated from d_{p1} to d_{p2} :

$$\ln \left(\frac{N(d_{p2})}{N(d_{p1})} \right) = \frac{d_0^2}{GR} \cdot \sum_j K(d_0, d_j) \cdot N_j \cdot \left(\frac{1}{d_{p2}} - \frac{1}{d_{p1}} \right). \quad (7)$$

Rearranging and solving for $N(d_{p1})$ yields:

$$N(d_{p1}) = N(d_{p2}) \cdot \exp \left(\frac{d_0^2}{GR} \cdot \sum_j K(d_0, d_j) \cdot N_j \cdot \left(\frac{1}{d_{p1}} - \frac{1}{d_{p2}} \right) \right) \quad (8)$$

10 or

$$N(d_{p1}) = N(d_{p2}) \cdot \exp \left(\frac{CS}{GR} \cdot d_0^2 \cdot \left(\frac{1}{d_{p1}} - \frac{1}{d_{p2}} \right) \right) \quad (9)$$

where

$$15 \quad CS = \sum_j K(1 \text{ nm}, d_j) \cdot N_j \quad (10)$$

is the condensation sink for 1 nm particles. The formation rates J can be obtained from the time-derivative of the particle number concentrations in Eq. (9). Although KK report a slightly different notation of Eq. (9), it is equivalent to their formulation.

and the particle diameter. At small particle sizes the Cunningham correction factor is approximately proportional to d_p^{-1} , and so the wall loss rate can be approximated by

$$k_w(d_p) = \frac{C'}{d_p} \quad (16)$$

5 where C' is an empirically-determined constant. Figure 1 shows the measured wall loss rate for the CLOUD chamber as a function of d_p (dashed curve, lower panel). The wall loss rate decreases as $\sim d_p^{-1}$, which is weaker than the assumed power dependency of $\sim d_p^{-2}$ for atmospheric particles (Eq. 5). Considering only wall losses an analytical solution for the correction factor can be obtained by adapting Eq. (4):

$$10 \frac{dN(d_p)}{N(d_p)} = -\frac{1}{GR} \cdot \frac{C'}{d_p} \cdot dd_p. \quad (17)$$

In this case integration yields:

$$\ln\left(\frac{N(d_{p2})}{N(d_{p1})}\right) = -\frac{C'}{GR} \cdot \ln\left(\frac{d_{p2}}{d_{p1}}\right) \quad (18)$$

15 OR

$$N(d_{p1}) = N(d_{p2}) \cdot \exp\left(\frac{C'}{GR} \cdot \ln\left(\frac{d_{p2}}{d_{p1}}\right)\right). \quad (19)$$

20 According to the example in Fig. 1, the value of C' is approximately 0.001 nm s^{-1} . Using again a growth rate of 3.6 nm h^{-1} , comparison between Eqs. (9) and (19) yields a 1.43 higher factor when wall loss is the dominant particle removal process (see also the dashed green curve in Fig. 2). However, if the growth rate becomes smaller, or for chambers with higher wall loss rates, then this factor rapidly increases, e.g. the discrepancy becomes ~ 35 at $C'/GR = 10$. In conclusion, the KK method cannot be applied in

On the derivation of particle nucleation rates from experimental formation rates

A. Kürten et al.

Title Page

Abstract

Introduction

Conclusions

References

Tables

Figures

◀

▶

◀

▶

Back

Close

Full Screen / Esc

Printer-friendly Version

Interactive Discussion



any environment other than one where the dominant losses are due to collisions with large pre-existing particles (i.e. atmospheric measurements and certain seed-particle chamber experiments). Furthermore, experiments and atmospheric environments with similar condensation sink rates cannot be directly compared before corrections are applied, because not only is the magnitude of the condensation sink important but also the dependency of the loss rate as function of particle size.

2.4 Universal method to derive the nucleation rate from the experimental formation rate

We will assume that the size distribution above a certain threshold size (d_{p2}) is known, using a Scanning Mobility Particle Sizer (SMPS) system with n size bins. For the following discussion it is useful to add m to all bin indices, although the original size distribution contains n size bins ranging from 1 to n . In this case the size d_{p2} corresponds to the bin with the index $m + 1$ (Fig. 3). The formation rate of particles at and above d_{p2} can then be calculated from:

$$J_{m+1} = \frac{dN_t}{dt} + \sum_{i=m+1}^{n+m} (k_w(d_{p,i}) \cdot N_i) + k_{dil} \cdot N_t + \sum_{i=m+1}^{n+m} \left(\sum_{j=i}^{n+m} \delta_{ij} \cdot K(d_{p,i}, d_{p,j}) \cdot N_j \cdot N_i \right) \quad (20)$$

where double-counting of collisions between particles in the same size bin is avoided by the factor (Seinfeld and Pandis, 2006):

$$\delta_{ij} = \begin{cases} 0.5 & \text{if } i = j \\ 1 & \text{if } i \neq j \end{cases} \quad (21)$$

The first term on the RHS takes into account non steady-state conditions, by the time derivative of the total particle number density N_t (sum of the particle concentrations from bin $m + 1$ to $n + m$). The remaining three terms on the RHS describe the loss processes of neutral particles in a chamber experiment: wall loss, loss due to dilution of

On the derivation of particle nucleation rates from experimental formation rates

A. Kürten et al.

Title Page

Abstract

Introduction

Conclusions

References

Tables

Figures

◀

▶

◀

▶

Back

Close

Full Screen / Esc

Printer-friendly Version

Interactive Discussion



In this equation all quantities are known except the value of N_m , which can be found after solving the quadratic equation (note that the last term on the RHS is quadratic in N_m). Once N_m is found the formation rate J_m can be calculated and the process can be repeated with the next smaller size bin (index $m - 1$). In this way the complete particle spectrum above d_{p1} (containing now $n + m$ size bins) can be recreated until the final formation rate $J_{d_{p1}}$ (at index 1) is calculated. The underlying assumption is that growth above this size is purely kinetic (no evaporation), which is fulfilled due to the assumption that d_{p1} is above the critical size.

In order to test the relative importance of coagulation – including self-coagulation – on the magnitude of the formation rate correction it is also possible to omit the last term on the RHS of Eq. (25). We will discuss in Sect. 3.3 under which circumstances this can be done without sacrificing too much accuracy.

2.5 Kinetic model for testing the universal method

A numerical model has been developed recently for the CLOUD chamber to simulate the formation and growth of uncharged sulfuric acid-dimethylamine particles (Kürten et al., 2014). The model assumes that particles grow from monomers by condensation and coagulation. Due to the arguments presented by Kürten et al. (2014), it has been concluded that $\text{H}_2\text{SO}_4 \cdot (\text{CH}_3)_2\text{NH}$ clusters (abbreviated as SA · DMA) constitute the basic “monomer” for the formation of particles in a system of sulfuric acid (SA) and dimethylamine (DMA). Assuming unit sticking efficiency and zero evaporation rate, good agreement is found between the model and the experimentally-measured neutral clusters.

The kinetic model is based on McMurry (1980). The time-dependent balance equation for the monomer concentration N_1 is

$$\frac{dN_1}{dt} = P_1 - \left(k_{1,w} + k_{\text{dil}} + \sum_{j=1}^N K_{1,j} \cdot N_j \right) \cdot N_1 \quad (26)$$

and, for all larger clusters ($k \geq 2$),

$$\frac{dN_k}{dt} = \frac{1}{2} \cdot \sum_{i+j=k} K_{i,j} \cdot N_i \cdot N_j - \left(k_{w,k} + k_{dil} + \sum_{j=1}^N K_{k,j} \cdot N_j \right) \cdot N_k. \quad (27)$$

Here, P_1 is the production rate of the monomers, k_w is the wall loss rate, k_{dil} the dilution rate, and K the coagulation coefficient.

The original model calculated concentrations of clusters ranging from dimer up to clusters of several thousand molecules. Each size bin was represented by a single cluster with a fixed number of molecules (or SA-DMA clusters, which are each treated as one molecule). The maximum particle size that can be reached with reasonable computation time is a few nm, which is too small for the current study. Therefore we adopted the method of Lovejoy et al. (2004) and incremented the size by one molecule for the first 30 bins (linear bins), and by a constant geometrical factor for the next 150 bins (geometric bins). By this method, a size of 60 nm can be reached using a geometrical factor of 1.023, which is suitable for the present study.

3 Discussion

Figure 4 shows the result of the kinetic model simulation for a monomer (molecular weight of 143 g mol^{-1} and density of 1.47 g cm^{-3}) production rate of $8.8 \times 10^4 \text{ cm}^{-3} \text{ s}^{-1}$, after $1.5 \times 10^4 \text{ s}$. Integration of Eqs. (26) and (27) yields the displayed size distribution (grey sticks). Although the particles continue to grow, the populations at smaller sizes (below about 10 nm) are close to steady-state. Since the total particle number concentration is dominated by these smaller particles, time-dependency can be neglected in the following, but will be revisited in Sect. 3.2. The size distribution (grey sticks in Fig. 4) is obtained after normalizing the concentrations by the number of SA molecules per bin.

On the derivation of particle nucleation rates from experimental formation rates

A. Kürten et al.

Title Page

Abstract

Introduction

Conclusions

References

Tables

Figures

◀

▶

◀

▶

Back

Close

Full Screen / Esc

Printer-friendly Version

Interactive Discussion



On the derivation of particle nucleation rates from experimental formation rates

A. Kürten et al.

Title Page

Abstract

Introduction

Conclusions

References

Tables

Figures

◀

▶

◀

▶

Back

Close

Full Screen / Esc

Printer-friendly Version

Interactive Discussion

The new universal method to derive a particle formation rate at a smaller size d_{p1} has been applied to the data shown in Fig. 4. A threshold size $d_{p2} = 3.2$ nm (corresponding to 2.9 nm geometric diameter) has been chosen. Starting with the size distribution for particles equal to or larger than 2.9 nm, 36 new bins were introduced to reach the size d_{p1} at 1.7 nm (1.4 nm geometric diameter). The red line shows the recreated size distribution obtained by this method. A constant growth rate of 3.92 nm h⁻¹ was chosen, corresponding to the value given by a numeric model calculation for a particle in the size bin m . As can be seen, the reconstruction works well for the first few size bins and then starts to deviate somewhat from the correct values. This occurs since the GR is not exactly constant with size, and slightly increases when approaching d_{p1} (see Sect. 3.1). If the true growth rate as a function of size is used, the reconstruction exactly reproduces the generated size distribution (see next section).

3.1 Size-dependent growth rate

The growth rate for a particle of size d_p can be calculated from (Lehtinen et al., 2007)

$$\text{GR}(d_p) = J(d_p) \cdot \frac{\Delta d_p}{N(d_p)} \quad (28)$$

Our studies with the kinetic model indicate that GR is only weakly-dependent on particle size in the range between critical size and detection threshold. In the example shown in Fig. 4 there is less than 20 % variation. However, the model does not include the effects of evaporation or of a spectrum of condensable vapors with different volatilities. Therefore care has to be taken when applying size corrections to atmospheric particle formation rates. The GR should ideally be measured over a wide range of diameters (Kulmala et al., 2013). In this case analytical solutions for the KK method can be found for certain size-dependent GRs (Korhonen et al., 2014). These considerations underscore the importance of directly measuring the particle GR in the sub-3 nm size range, as well as at larger sizes. With this information the effect of particle evaporation

can be separated from the uncertainties due to size-dependent particle GR. In the absence of such measurements, a detailed error analysis is required to bracket the range of GR uncertainty and its impact on the derived nucleation rates.

When using the size-dependent growth rate in the reconstruction method, by updating the GR in Eq. (25) at each step, perfect agreement between the generated and reconstructed size distributions can be achieved (blue line in Fig. 4). A comparison between using a constant GR and a size-dependent GR is also shown in Fig. 5. Here, the formation rates are compared as function of size. The accurate solution from the kinetic model is shown by the black solid line, while the results from the reconstruction method are indicated by the symbols. Again, perfect agreement is reached when using a size-dependent GR (blue triangles), while a constant GR (red circles) leads to an over-estimation of the formation rate by $\sim 40\%$ at the smallest size.

3.2 Time evolution in a simulated chamber nucleation experiment

Using the kinetic model, we show in Fig. 6 an example of the time-dependent formation rates J (black lines) for the particle sizes d_{p1} (1.4 nm geometric diameter; solid lines) and d_{p2} (2.9 nm geometric diameter; dashed lines). In addition, the rate of change of particle concentration dN/dt (blue lines) above the size thresholds d_{p1} and d_{p2} are shown. The formation rates J are directly obtained from the model using Eq. (25) and the size distribution. Interestingly, the formation rates overshoot before they reach an almost constant value. This overshoot is explained by the absence of larger particles at the beginning of the experiment. Therefore the loss rate is smaller at the beginning, which allows for faster formation rates. Once the larger particles start to form, the loss rate increases until eventually there are only small changes in particle concentrations and formation rates. This overshoot can be quite large and, in this example, reaches almost a factor of three for the maximum J compared with its steady-state value.

Using the size distribution as a function of time for particle sizes equal to or larger than d_{p2} (not shown), as well as the growth rates $GR(d_{p2})$ (not shown) and the time

On the derivation of particle nucleation rates from experimental formation rates

A. Kürten et al.

Title Page

Abstract

Introduction

Conclusions

References

Tables

Figures

◀

▶

◀

▶

Back

Close

Full Screen / Esc

Printer-friendly Version

Interactive Discussion

On the derivation of particle nucleation rates from experimental formation rates

A. Kürten et al.

Title Page

Abstract

Introduction

Conclusions

References

Tables

Figures

◀

▶

◀

▶

Back

Close

Full Screen / Esc

Printer-friendly Version

Interactive Discussion



derivative of the total ($\geq d_{p2}$) number concentration of particles $dN(d_{p2})/dt$, the size-corrected formation rate $J(d_{p1})$ can be derived by the method described above (red line). The derived formation rate agrees closely with the accurate solution from the kinetic model (black solid line) for conditions close to steady-state. However, when evaluating J at d_{p1} from the formation rate at d_{p2} and time t one needs to consider that the particles that appear at d_{p2} were passing the size d_{p1} at an earlier time t' . This time can be approximated by

$$t' = t - \frac{d_{p2} - d_{p1}}{\text{GR}} \quad (29)$$

if the time and size-dependency of the GR is neglected. The over-estimation (difference between the red and black lines in Fig. 6) is due to the size-dependency of the growth rate (see previous section). An accurate determination of $J(d_{p1})$ can only be obtained after the particle formation rate at d_{p2} has reached steady-state. This is reached when the rate of change of particle concentration (dashed blue line in Fig. 6) approaches zero.

3.3 Formation rates as function of the sulfuric monomer concentration

In the preceding section, the universal method has only been tested for one sulfuric acid monomer concentration. Variation of the monomer production rate P in Eq. (26) will result in different sulfuric acid concentrations. The resulting size distributions (N), growth rates (GR) and rates of change of particle concentration (dN/dt) as a function of particle size can be used to test the reconstruction method. Figure 7 shows the results for 5×10^5 to $2 \times 10^7 \text{ cm}^{-3}$ sulfuric acid concentration. The accurate solution for d_{p2} is shown by the green solid line. Using a size-dependent GR the universal method (blue solid line) yields identical values as the kinetic model for $J(d_{p1})$ (dashed magenta line). However, if a constant GR is used, corresponding to its value at d_{p2} , then $J(d_{p1})$ (red solid line) is over-estimated since, for this system, the GR increases slightly with decreasing size.

a given experiment (around $100 \text{ cm}^{-3} \text{ s}^{-1}$ in the case of CLOUD), it can be neglected for all smaller formation rates in any chemical system.

4 Conclusions

The Kerminen and Kulmala (2002) method is widely used in atmospheric and chamber experiments to derive nucleation rates from experimentally-measured formation rates at larger particle sizes. However, we have shown that the applicability of the KK method is limited to cases where the dominant particle losses are due to coagulation with large pre-existing particles, and that significant inaccuracies can result for most chamber experiments, where the loss rates have different size-dependencies.

We have therefore presented a new universal method that yields representative results in any general environment, provided certain quantities are known. The new method requires knowledge of the particle size spectrum above the detection threshold, the particle growth rate, and all loss processes as a function of particle size. With this information the size spectrum and the formation rate can be reconstructed in a step-wise process to a smaller size, where the nucleation rate is determined. The universal method can give accurate results and, furthermore, takes into account self-coagulation among newly-formed particles, which can be an important effect, recognized previously by Anttila et al. (2010). Additionally, if the size-dependent growth rate is available from measurements, it can be readily incorporated during the reconstruction of the size distribution.

The proposed new method allows extrapolation of the particle formation rate measured at one threshold size to a second, smaller size. In this way, a precise quantitative comparison can be made between formation rates measured simultaneously by several counters operating in the 1 to 3 nm threshold range and, where differences emerge, a deeper understanding of fundamental quantities such as cluster critical sizes, growth rates and evaporation rates can be obtained.

**On the derivation of
particle nucleation
rates from
experimental
formation rates**

A. Kürten et al.

[Title Page](#)[Abstract](#)[Introduction](#)[Conclusions](#)[References](#)[Tables](#)[Figures](#)[◀](#)[▶](#)[◀](#)[▶](#)[Back](#)[Close](#)[Full Screen / Esc](#)[Printer-friendly Version](#)[Interactive Discussion](#)

position dependent response of a nano-CPC battery, *Atmos. Meas. Tech.*, 7, 689–700, doi:10.5194/amt-7-689-2014, 2014.

Kerminen, V. M. and Kulmala, M.: Analytical formulae connecting the “real” and the “apparent” nucleation rate and the nuclei number concentration for atmospheric nucleation events, *J. Aerosol Sci.*, 33, 609–622, 2002.

Kirkby, J., Curtius, J., Almeida, J., Dunne, E., Duplissy, J., Ehrhart, S., Franchin, A., Gagné, S., Ickes, L., Kürten, A., Kupc, A., Metzger, A., Riccobono, F., Rondo, L., Schobesberger, S., Tsagkogeorgas, G., Wimmer, D., Amorim, A., Bianchi, F., Breitenlechner, M., David, A., Dommen, J., Downard, A., Ehn, M., Flagan, R. C., Haider, S., Hansel, A., Hauser, D., Jud, W., Junninen, H., Kreissl, F., Kvashin, A., Laaksonen, A., Lehtipalo, K., Lima, J., Lovejoy, E. R., Makhmutov, V., Mathot, S., Mikkilä, J., Minginette, P., Mogo, S., Nieminen, T., Onnela, A., Pereira, P., Petäjä, T., Schnitzhofer, R., Seinfeld, J. H., Sipilä, M., Stozhkov, Y., Stratmann, F., Tomé, A., Vanhanen, J., Viisanen, Y., Vrtala, A., Wagner, P. E., Walther, H., Weingartner, E., Wex, H., Winkler, P. M., Carslaw, K. S., Worsnop, D. R., Baltensperger, U., and Kulmala, M.: Role of sulphuric acid, ammonia and galactic cosmic rays in atmospheric aerosol nucleation, *Nature*, 476, 429–435, 2011.

Korhonen, H., Kerminen, V.-M., Kokkola, H., and Lehtinen, K. E. J.: Estimating atmospheric nucleation rates from size distribution measurements: analytical equations for the case of size dependent growth rates, *J. Aerosol Sci.*, 69, 13–20, 2014.

Kuang, C., Chen, M., McMurry, P. H., and Wang, J.: Modification of laminar flow ultrafine condensation particle counters for the enhanced detection of 1 nm condensation nuclei, *Aerosol Sci. Tech.*, 46, 309–315, 2012a.

Kuang, C., Chen, M., Zhao, J., Smith, J., McMurry, P. H., and Wang, J.: Size and time-resolved growth rate measurements of 1 to 5 nm freshly formed atmospheric nuclei, *Atmos. Chem. Phys.*, 12, 3573–3589, doi:10.5194/acp-12-3573-2012, 2012b.

Kulmala, M., Vehkamäki, H., Petäjä, T., Dal Maso, M., Lauri, A., Kerminen, V.-M., Birmili, W., and McMurry, P. H.: Formation and growth rates of ultrafine atmospheric particles: a review of observations, *J. Aerosol Sci.*, 35, 143–176, 2004.

Kulmala, M., Kontkanen, J., Junninen, H., Lehtipalo, K., Manninen, H. E., Nieminen, T., Petäjä, T., Sipilä, M., Schobesberger, S., Rantala, P., Franchin, A., Jokinen, T., Järvinen, E., Äijälä, M., Kangasluoma, J., Hakala, J., Aalto, P. P., Paasonen, P., Mikkilä, J., Vanhanen, J., Aalto, J., Hakola, H., Makkonen, U., Ruuskanen, T., Mauldin III, R. L., Duplissy, J., Vehkamäki, H., Bäck, J., Kortelainen, A., Riipinen, I., Kurtén, T., Johnston, M. V., Smith, J. N.,

**On the derivation of
particle nucleation
rates from
experimental
formation rates**

A. Kürten et al.

Title Page

Abstract

Introduction

Conclusions

References

Tables

Figures

◀

▶

◀

▶

Back

Close

Full Screen / Esc

Printer-friendly Version

Interactive Discussion

Ehn, M., Mentel, T. F., Lehtinen, K. E. J., Laaksonen, A., Kerminen, V.-M., Worsnop, D. R.: Direct observations of atmospheric aerosol nucleation, *Science*, 339, 943–946, 2013.

5 Kürten, A., Jokinen, T., Simon, M., Sipilä, M., Sarnela, N., Junninen, H., Adamov, A., Almeida, J., Amorim, A., Bianchi, F., Breitenlechner, M., Dommen, J., Donahue, N. M., Duplissy, J., Ehrhart, S., Flagan, R. C., Franchin, A., Hakala, J., Hansel, A., Heinritzi, M., Hutterli, M., Kangasluoma, J., Kirkby, J., Laaksonen, A., Lehtipalo, K., Leiminger, M., Makhmutov, V., Mathot, S., Onnela, A., Petäjä, T., Praplan, A. P., Riccobono, F., Rissanen, M. P., Rondo, L., Schobesberger, S., Seinfeld, J. H., Steiner, G., Tomé, A., Tröstl, J., Winkler, P. M., Williamson, C., Wimmer, D., Ye, P., Baltensperger, U., Carslaw, K. S., Kulmala, M., Worsnop, D. R., and Curtius, J.: Neutral molecular cluster formation of sulfuric acid-dimethylamine observed in real-time under atmospheric conditions, *Proc. Natl. Acad. Sci. USA*, 111, 15019–15024, doi:10.1073/pnas.1404853111, 2014.

10 Lehtinen, K. E. J., dal Maso, M., Kulmala, M., and Kerminen, V.-M.: Estimating nucleation rates from apparent particle formation rates and vice versa: revised formulation of the Kerminen–Kulmala equation, *J. Aerosol Sci.*, 38, 988–994, 2007.

15 Lovejoy, E. R., Curtius, J., and Froyd, K. D.: Atmospheric ion-induced nucleation of sulfuric acid and water, *J. Geophys. Res.*, 109, D08204, doi:10.1029/2003JD004460, 2004.

McMurry, P. H.: Photochemical aerosol formation from SO₂: a theoretical analysis of smog chamber data, *J. Colloid Interf. Sci.*, 78, 513–527, 1980.

20 McMurry, P. H., Fink, M., Sakurai, H., Stolzenburg, M. R., Mauldin III, R. L., Smith, J., Eisele, F., Moore, K., Sjostedt, S., Tanner, D., Huey, L. G., Nowak, J. B., Edgerton, E., and Voisin, D.: A criterion for new particle formation in the sulfur-rich Atlanta atmosphere, *J. Geophys. Res.*, 110, D22S02, doi:10.1029/2005JD005901, 2005.

25 Metzger, A., Verheggen, B., Dommen, J., Duplissy, J., Prevot, A. S. H., Weingartner, E., Riipinen, I., Kulmala, M., Spracklen, D. V., Carslaw, K. S., and Baltensperger, U.: Evidence for the role of organics in aerosol particle formation under atmospheric conditions, *Proc. Natl. Acad. Sci. USA*, 107, 6646–6651, 2010.

30 Riccobono, F., Schobesberger, S., Scott, C. E., Dommen, J., Ortega, I. K., Rondo, L., Almeida, J., Amorim, A., Bianchi, F., Breitenlechner, M., David, A., Downard, A., Dunne, E. M., Duplissy, J., Ehrhart, S., Flagan, R. C., Franchin, A., Hansel, A., Junninen, H., Kajos, M., Keskinen, H., Kupc, A., Kürten, A., Kvashin, A. N., Laaksonen, A., Lehtipalo, K., Makhmutov, V., Mathot, S., Nieminen, T., Onnela, A., Petäjä, T., Praplan, A. P., Santos, F. D., Schallhart, S., Seinfeld, J. H., Sipilä, M., Spracklen, D. V., Stozhkov, Y., Stratmann, F.,

On the derivation of particle nucleation rates from experimental formation rates

A. Kürten et al.

Title Page

Abstract

Introduction

Conclusions

References

Tables

Figures

◀

▶

◀

▶

Back

Close

Full Screen / Esc

Printer-friendly Version

Interactive Discussion



Tomé, A., Tsagkogeorgas, G., Vaattovaara, P., Viisanen, Y., Vrtala, A., Wagner, P. E., Weingartner, E., Wex, H., Wimmer, D., Carslaw, K. S., Curtius, J., Donahue, N. M., Kirkby, J., Kulmala, M., Worsnop, D. R., and Baltensperger, U.: Oxidation products of biogenic emissions contribute to nucleation of atmospheric particles, *Science*, 344, 6185, 717–721, 2014.

5 Seinfeld, J. H. and Pandis, S. N.: *Atmospheric Chemistry and Physics: from Air Pollution to Climate Change*, 2nd edn., John Wiley & Sons, Inc., Hoboken, NJ, 595-610, 2006.

Sgro, L. A. and Fernández de la Mora, J.: A simple turbulent mixing CNC for charged particle detection down to 1.2 nm, *Aerosol. Sci. Tech.*, 38, 1–11, 2004.

10 Vanhanen, J., Mikkilä, J., Lehtipalo, K., Sipilä, M., Manninen, H. E., Siivola, E., Petäjä, T., and Kulmala, M.: Particle size magnifier for nano-CN detection, *Aerosol Sci. Tech.*, 45, 533–542, 2011.

Weber, R. J., Marti, J. J., McMurry, P. H., Eisele, F. L., Tanner, D. J., and Jefferson, A.: Measurements of new particle formation and ultrafine particle growth rates at a clean continental site, *J. Geophys. Res.*, 102, 4375–4385, 1997.

15 Wimmer, D., Lehtipalo, K., Franchin, A., Kangasluoma, J., Kreissl, F., Kürten, A., Kupc, A., Metzger, A., Mikkilä, J., Petäjä, T., Riccobono, F., Vanhanen, J., Kulmala, M., and Curtius, J.: Performance of diethylene glycol-based particle counters in the sub-3 nm size range, *Atmos. Meas. Tech.*, 6, 1793–1804, doi:10.5194/amt-6-1793-2013, 2013.

On the derivation of particle nucleation rates from experimental formation rates

A. Kürten et al.

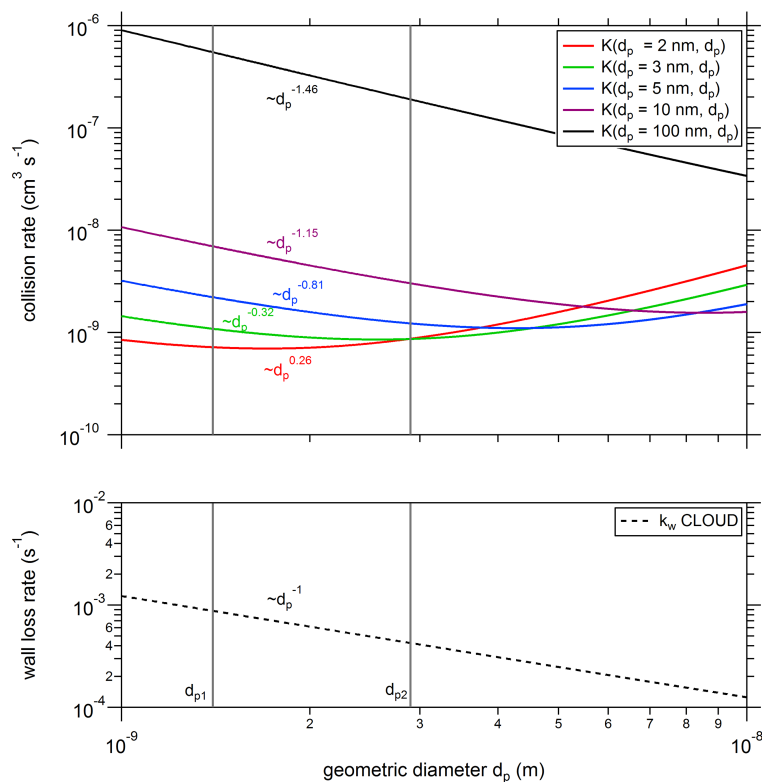


Figure 1. Collision rate, K , as function of particle size, d_p (upper panel). Collision rates are calculated between two particles where one particle has a constant size (indicated in the legend of the figure) and the second particle diameter varies between 1 and 10 nm. The wall loss rate for the CLOUD chamber as function of particle size is shown by the dashed curve (lower panel). Slopes of the curves are indicated for the range between d_{p1} (1.4 nm, i.e. 1.7 nm in mobility diameter) and d_{p2} (2.9 nm, i.e. 3.2 nm in mobility diameter).

On the derivation of particle nucleation rates from experimental formation rates

A. Kürten et al.

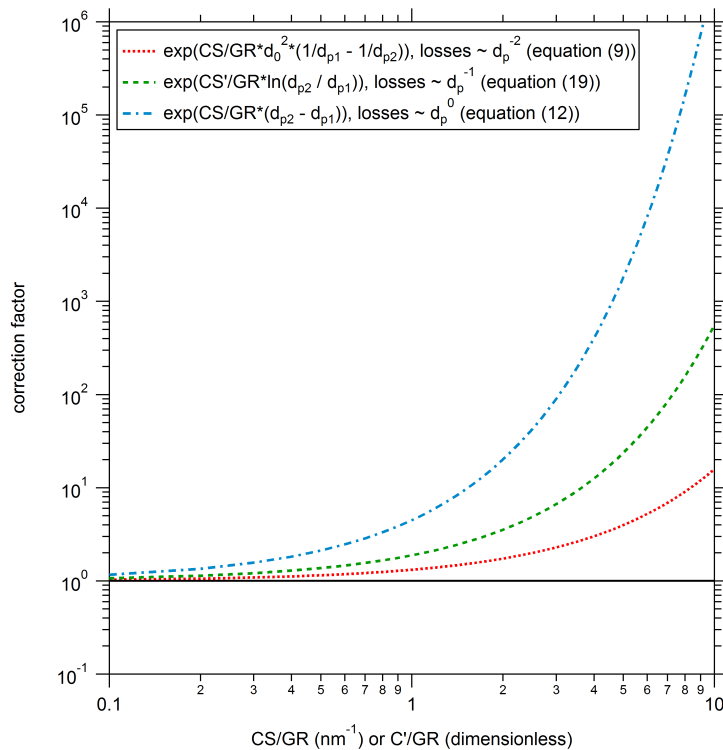


Figure 2. Correction factors calculated for different size-dependencies of the loss processes. The diameters used in the equations are $d_{p1} = 1.7$ nm and $d_{p2} = 3.2$ nm. See text for details.

On the derivation of particle nucleation rates from experimental formation rates

A. Kürten et al.

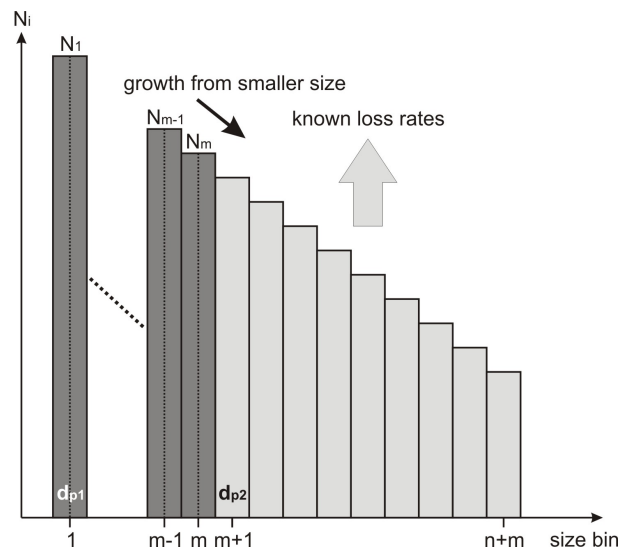


Figure 3. The original size distribution above the cut-off size d_{p2} (size bin $m + 1$) is shown in light gray. The loss rate of particles and the rate of change of the particle concentration in this size range must be compensated by the formation rate due to smaller particles growing into the measured size range. This knowledge can be incrementally extended to bins at smaller sizes in a step-wise process, finally reaching the smaller size, d_{p1} .

Title Page

Abstract

Introduction

Conclusions

References

Tables

Figures

◀

▶

◀

▶

Back

Close

Full Screen / Esc

Printer-friendly Version

Interactive Discussion

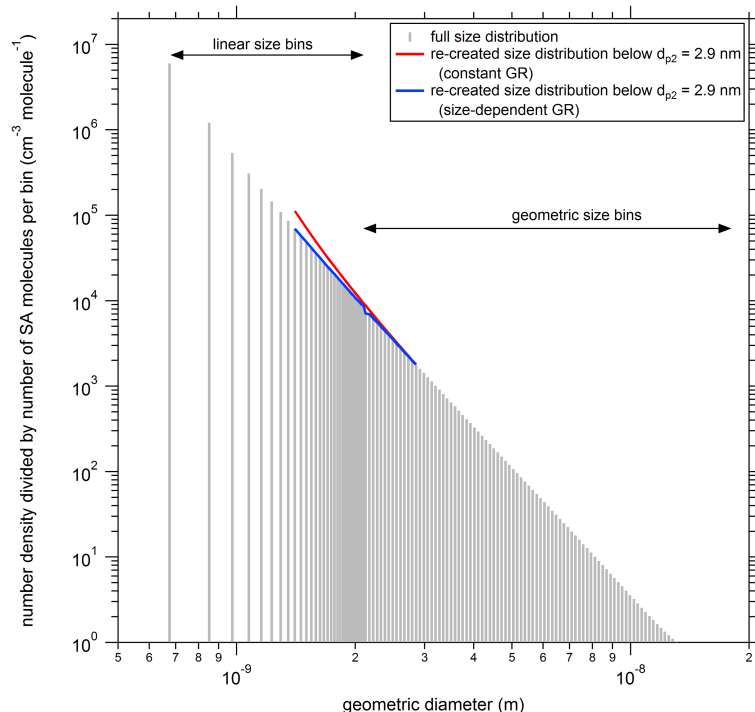


Figure 4. Modeled and reconstructed particle size distribution. The model uses different definitions for the first 30 size bins (up to ~ 2.1 nm) and the last 150 size bins ($\gtrsim 2.1$ nm). In the first 30 size bins, the number of molecules in the particles increases by one between each bin, whereas in the next 150 bins the particle diameter is increased by a constant factor between each bin. Normalizing the concentration by the number of molecules per bin leads to the shown size distribution (grey sticks). The reconstructed size distribution using the new method described here is shown by the solid lines, starting from the particle distribution above 2.9 nm. The solution using a size-dependent growth rate (GR) is shown by the blue line and, for a constant GR (taken at d_{p2}), by the red line.

On the derivation of particle nucleation rates from experimental formation rates

A. Kürten et al.

Title Page	
Abstract	Introduction
Conclusions	References
Tables	Figures
◀	▶
◀	▶
Back	Close
Full Screen / Esc	
Printer-friendly Version	
Interactive Discussion	



On the derivation of particle nucleation rates from experimental formation rates

A. Kürten et al.

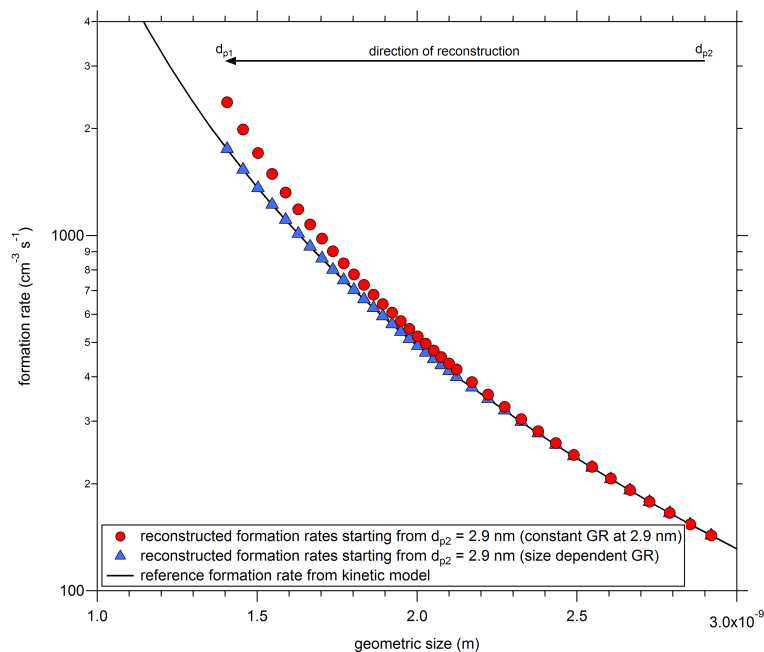


Figure 5. Formation rates as function of particle size. Formation rates simulated with the kinetic model are shown by the black line. Reconstructed particle formation rates starting at $d_{p2} = 2.9 \text{ nm}$ and ending at $d_{p1} = 1.4 \text{ nm}$ are shown by the blue triangles for a size-dependent growth rate (GR) and by the red circles for a constant GR (taken at d_{p1}).

On the derivation of particle nucleation rates from experimental formation rates

A. Kürten et al.

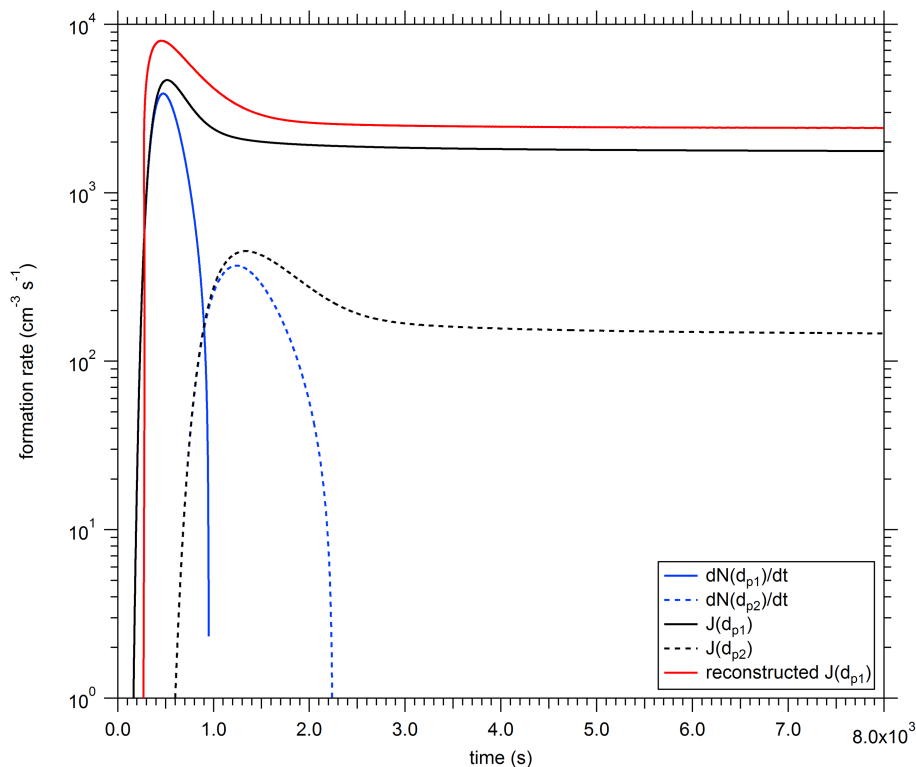


Figure 6. Particle formation rates J ($\text{cm}^{-3} \text{s}^{-1}$, black lines) and change in particle concentration dN/dt ($\text{cm}^{-3} \text{s}^{-1}$, blue lines) shown for two different sizes, $d_{p1} = 1.4 \text{ nm}$ (solid lines) and $d_{p2} = 2.9 \text{ nm}$ (dashed lines). The data are from a kinetic model calculation. The reconstructed $J(d_{p1})$ is shown by the red solid line.

[Title Page](#)[Abstract](#)[Introduction](#)[Conclusions](#)[References](#)[Tables](#)[Figures](#)[◀](#)[▶](#)[◀](#)[▶](#)[Back](#)[Close](#)[Full Screen / Esc](#)[Printer-friendly Version](#)[Interactive Discussion](#)

On the derivation of particle nucleation rates from experimental formation rates

A. Kürten et al.

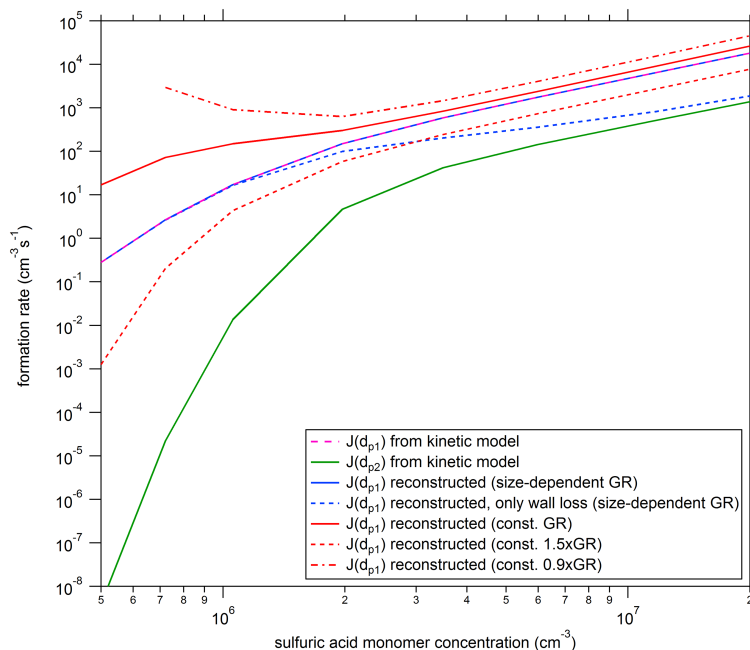


Figure 7. Formation rates as function of the sulfuric acid monomer concentration. The solid green curve shows the formation rate at d_{p2} calculated from the kinetic model. The simulated formation rates $J(d_{p1})$ from the kinetic model are indicated by the dashed magenta line. The reconstructed formation rates at d_{p1} using the size-dependent GRs are shown by the solid blue line, and agree well with the simulations. The solid red line shows the reconstructed formation rates at d_{p1} using a constant GR, evaluated at d_{p2} . Varying the constant GR by a factor of 1.5 and 0.9 results in the dashed and the dashed-dotted red curves, respectively. Neglecting coagulation but using a size-dependent GR yields the dashed blue line.

Title Page

Abstract

Introduction

Conclusions

References

Tables

Figures

◀

▶

◀

▶

Back

Close

Full Screen / Esc

Printer-friendly Version

Interactive Discussion